Inorganic Chemistry

pubs.acs.org/IC

Communication

Solvent Effects on the Phosphorescence of Gold(III) Complexes Chelated by β-Multisubstituted Corroles

Xuan Zhan, Woohyun Lee, Kolanu Sudhakar, Donghyeon Kim, Atif Mahammed,* David G. Churchill,* and Zeev Gross*

Cite This: *Inorg. Chem.* 2021, 60, 8442−8446

Read Online

ACCESS | Metrics & More | Article Recommendations | Supporting Information

ABSTRACT: A set of gold corrole complexes containing four different β-substituent groups (Br/I/CF_3), namely, **4Br−Au**, **4I−Au**, and **4CF_3−Au**, were investigated; all showed room temperature phosphorescence. The phosphorescence quantum yields of the corroles were determined using tetraphenylporphyrin as a reference: Φ_{ph} (**4I−Au**, 0.75%) > Φ_{ph} (**4Br−Au**, 0.64%) > Φ_{ph} (**4CF_3-Au**, 0.38%). **4CF_3−Au** exhibited near-IR emission (858 nm, aerobic); absorbance intensity for the Q-band was higher than that for the Soret band. Complex **4I−Au** showed a longer phosphorescence lifetime (82 μs) compared to those of **4Br−Au** (53 μs) and **4CF_3−Au** (28 μs; N_2, tol). Thermally activated delayed fluorescence (TADF) emission of **4I/Br−Au** complexes was observed: stronger emission intensity correlated with increasing temperature. Good negative correlations for **4I/Br−Au** were observed between the Soret band absorption energy and the solvent polarizability: excited states of **4I/Br−Au** are more polar than their ground states. TD-DFT calculations revealed very fast intersystem crossing (ISC) rate constants, 2.20×10^{12} s^{-1} (**4CF_3−Au**) > 1.96×10^{11} s^{-1} (**4Br−Au**) > 1.15×10^{11} s^{-1} (**4I−Au**), and importantly, the reverse intersystem crossing (rISC) rate constants are determined as 1.68×10^{7} s^{-1} (**4I−Au**) > 2.40×10^{3} s^{-1} (**4Br−Au**) ≫ 8.09×10^{-8} s^{-1} (**4CF_3−Au**). The exceptionally low rISC rate constant of **4CF_3−Au** is attributed to its more steric and deformed structure bearing a larger energy gap between the S_1 and T_1 states.

As part of the synthesis, analysis, and other determinations, solvent systems and incident light are important factors for corrole research[1,2] of importance. We and others have undertaken the synthesis of corrole complexes with 5d metals such as W,[3] Re,[4] Ir,[5] Au,[6] and Os.[7] Photophysical and catalytic investigations have demonstrated that gold(III) corrole complexes are potentially excellent candidates for versatile applications due to their unique photophysical properties such as near-IR phosphor oxygen sensing,[8] potent pharmaceutical cytotoxic and cytostatic agent administering,[9] and efficient photosensitizing in organic solar cells.[10] Their room temperature near-IR phosphorescence is perhaps currently the most noteworthy photophysical property arousing current and continued interest.

Different analogues and isomers of corrole β-multisubstituted species involving bromination,[11] iodination,[12] and CF_3 group incorporation are important to explore.[13,6c] The substitution pattern, as well as the symmetry of the resulting dye, also comes into play regarding the in-depth study of the molecular photophysical properties.

Solvent effects are important in regulating charge transfer processes of metal complexes;[14] spectroelectrochemical studies of transition metal corrole complexes have been widely probed.[15−19] However, little literature was uncovered on the *solvent effect* on corrole *phosphorescence*, prompting us to investigate photophysical signatures imparted by gold corroles. Our study herein focuses on the solvent effect on the absorption spectra, the phosphorescence intensity and lifetime, and the newly observed phenomenon of delayed fluorescence in gold corroles.

Experimental Study. Three 2,3,17,18-substituted corroles, namely, tetra-β-brominated/iodinated/trifluoromethylated gold corroles (Figure 1a), were prepared by way of previously published protocols.[6] Typical near-UV (Soret) and far-visible (Q) bands were observed (Figure 1b). **4I−Au** exhibited the most red-shifted absorption spectrum; Soret and Q-band maxima are at 417 and 578 nm, respectively. Intermediate absorption red-shifting was observed for the tetra-*brominated* complex (**4Br−Au**; Soret band, 413 nm; Q-band, 575 nm) and significantly more than for the tetra-CF_3 substituted species (**4CF_3−Au**; Soret band and Q-band at 403 and 572 nm). By comparison, β-iodination is, therefore, an effective approach to help the induction of absorption red-shifting for these tetra-substituted species. Noticeably, a larger Q-band absorbance coefficient constant ($\varepsilon = 7.59 \times 10^4$ $L{\cdot}mol^{-1}cm^{-1}$) for **4CF_3−Au** was observed, compared to the Soret band absorption coefficient constant ($\varepsilon = 5.69 \times 10^4$ $L{\cdot}mol^{-1}cm^{-1}$). The phosphorescence quantum yields of the studied gold corroles were determined using tetraphenylporphyrin as a standard (H_2TPP, $\Phi_f = 0.13$ in toluene at 298 K and N_2 atmosphere): Φ_{ph} (**4I−Au**, 0.75%) > Φ_{ph} (**4Br−Au**, 0.64%) > Φ_{ph} (**4CF_3-Au**, 0.38%). The Φ_{ph} of 0.38−0.75% is consistent with earlier literature reports.[6,8,10] Considering the presence of multiple

Received: March 25, 2021
Published: June 10, 2021

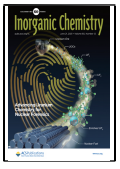

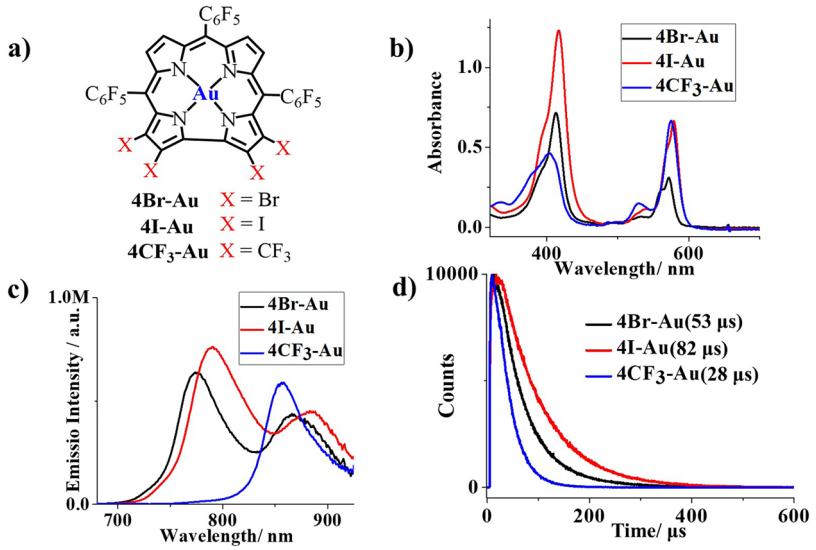

Figure 1. (a) Corroles studied herein. (b) UV−vis spectra of corroles in acetonitrile (1.0×10^{-5} M) at room temperature. (c) Comparison of corrole phosphorescence emission spectra under a N_2 atmosphere in toluene (1.0×10^{-6} M) at room temperature under different excitation wavelengths: λ_{ex} (**4Br−Au**) = 572 nm, λ_{ex} (**4I−Au**) = 578 nm, and λ_{ex} (**$4CF_3$−Au**) = 575 nm.[6d−f] (d) Comparison of time−resolved phosphorescence decay curves (μs, microseconds) of three gold corroles under a N_2 atmosphere and room temperature, excitation wavelength same as in c.

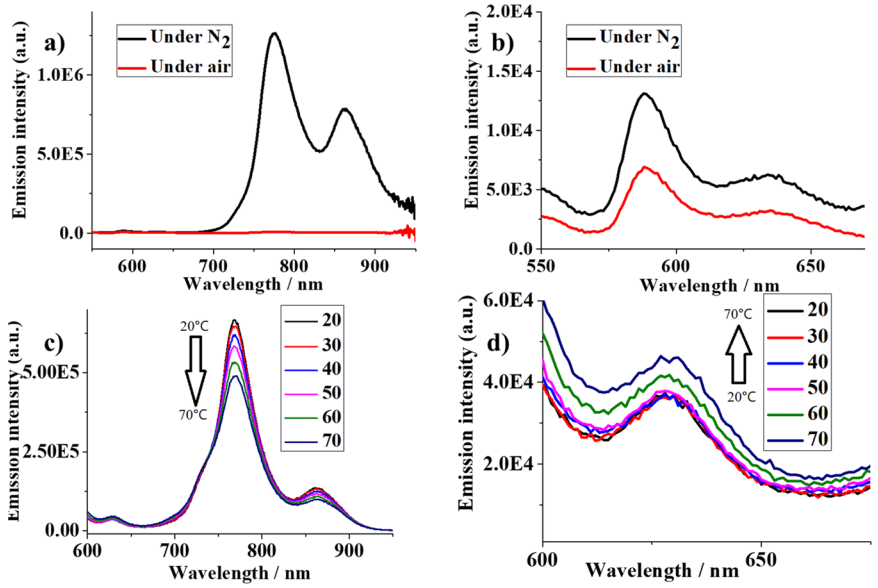

Figure 2. (a) Emission spectra of **4Br−Au** in toluene. (b) Enlarged area from (a) focusing the wavelength ranging from 550 to 650 nm. (c) Temperature dependent emission spectra (°C) of **4Br−Au** recorded in toluene. (d) Enlarged area (600−670 nm) from c.

heavy atoms (gold and halides) and also the large Stokes shifts of 200−270 nm, the yields may actually be considered relatively high.

The phosphorescence emission spectra of the corroles were recorded (Figure 1c). Surprisingly, **$4CF_3$−Au** displayed a red-shifted near-IR spectrum (λ_{em} = 858 nm); the corresponding phosphorescence emission peaks for **4Br−Au** and **4I−Au** were found at 775 and 790 nm, respectively. **$4CF_3$−Au** is characterized by the most *blue-shifted* absorbance (403 nm) and the most *red-shifted* emission (858 nm), giving rise to an extraordinarily large Stokes shift (455 nm). We, therefore, hypothesize that the CF_3 group has a pronounced steric effect that apparently is strongly affected by its own photoexcitation. Furthermore, **4I−Au** exhibited the longest lifetime (82 μs) followed by the tetra-brominated species **4Br−Au** (53 μs) and then by **$4CF_3$−Au** (28 μs). The shorter phosphorescence lifetime for **$4CF_3$−Au** is explained by the sterics of the β-trifluoromethylated species; **$4CF_3$−Au** possesses a much more distorted macrocycle than the β-halogenated species does (**4I−Au** and **4Br−Au**).[6c] The excitation, absorbance, and emission spectra were well compared as depicted in Figure S1 exemplified with species **4I−Au**, which exhibited a miniscule fluorescence emission at 640 nm.

Microsecond lifetimes were not the only indication for the measured emission to reflect phosphorescence. The presence of air [O_2] completely quenches the electronic emission (Figure 2a). However, the much less intense emission centered at ∼600 nm was not efficiently quenched (Figure 2b). The

https://doi.org/10.1021/acs.inorgchem.1c00906
Inorg. Chem. 2021, 60, 8442−8446

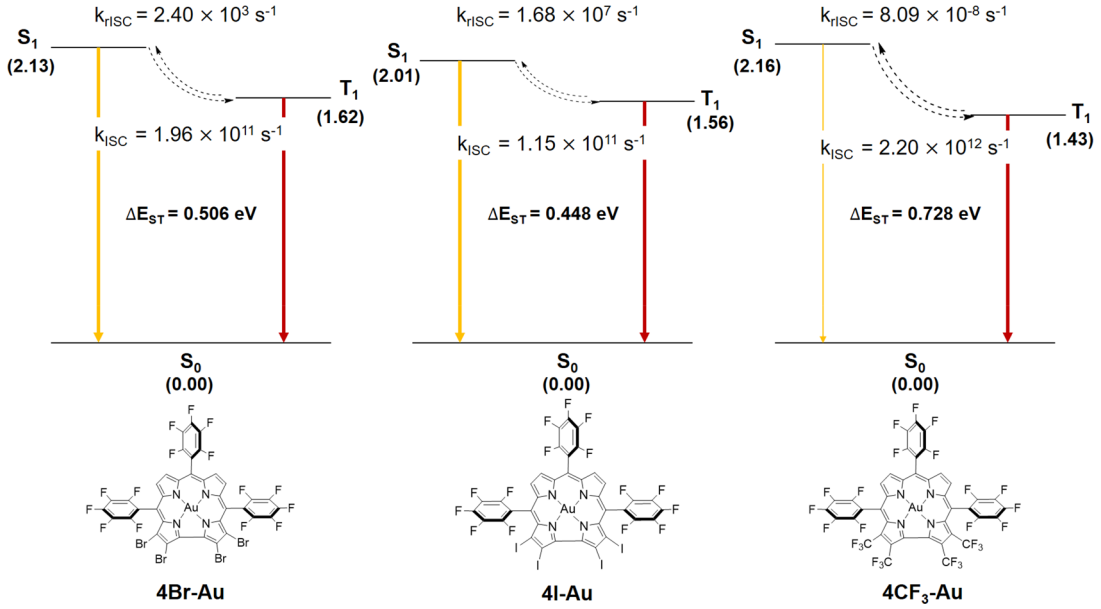

Figure 3. Schematic energy (electron volts) diagram emission in gold corrole complexes **4Br−Au**, **4I−Au**, and **4CF$_3$−Au**. Fluorescence = (yellow) and phosphorescence = (red).

main (700−900 nm) and minor emissions (600−650 nm) also did not respond identically to changes in temperature. Instead, they decreased and increased, respectively, from 20 to 70 °C (Figure 2c and d), reflecting the delayed fluorescence characteristic. The similar change in the temperature-dependence intensity was also found for **4I−Au** (Figure S7), which featured thermally activated delayed fluorescence (TADF) at around 640 nm. Fluorescence lifetimes were measured as exemplified by the case of **4I−Au**, slow decay at 640 nm: $\tau_1(N_2)$ (μs) = 10.06 (Rel = 86.90%), $\tau_2(N_2)$ (μs) = 132.92 (Rel = 13.10%). Fast decay at 640 nm: $\tau_1(N_2)$ (ns) = 0.35 (Rel = 30.30%), $\tau_2(N_2)$ (ns) = 3.84 (Rel = 69.70%; data provided in the Supporting Information, Figures S2, S3). Thus, weak prompt fluorescence and strong phosphorescence were detected from **4Br−Au** and **4I−Au**, and the TADF was also observed and determined.

Solvent effects were investigated, as exemplified in the case of **4I−Au** (Figure S4); 11 different solvents were investigated.[6d−f] Polarizability is defined as[20]

$$F(n) = (n^2 - 1)/(2n^2 + 1) \quad (1)$$

in which n is the measured refractive index of the solvent recorded at 20 °C. The plot of the Soret band allows the formation of a maximum against $F(n)$ to be linearly fitted to the equation in Figure S4.

The negative correlation, between the Soret band absorption energy and the solvent polarizability, observed in the case of **4Br−Au** but not for **4CF$_3$−Au** (Figures S8 and S9), demonstrates that the excited states of **4I/Br−Au** are more polar than their ground states.[21] The solvent effect studies on the excited states of small aromatic molecules such as butyrophenone,[22] thioxanthone,[23] and nitrobenzaldehyde[24] suggest that the increased solvent polarity acts to decrease the electronic $S-T$ intersystem crossing process and induce the rise of $^3(n,\Pi^*)$ and suppression of $^3(\Pi,\Pi^*)$; manifested in $^3(\Pi,\Pi^*)$ is an observed lifetime, longer than $^3(n,\Pi^*)$. The solvent-dependent phosphorescence emission spectrum of **4I−Au** was then examined (Figure S5): besides a similar shape, the phosphorescence spectrum (λ_{max} = 790 nm) reaches a maximum value in toluene, decreasing evenly by the increasing polarity of the solvent. A similar phosphorescence intensity decrease pattern was observed for **4Br−Au** and **4CF$_3$−Au** (Figures S7 and S8). Interestingly, the delayed fluorescence of complex **4I−Au** centered at around 640 nm exhibited insensitivity to solvent change, which only showed a bit higher intensity when measured in DMF (Figure S5, right).

Another parameter correlating with solvent influence is *phosphorescence lifetime*. As suggested previously, the intersystem crossing process is diminished with increasing solvent polarity;[21] this lifetime is expected to shorten with greater polarity of solvent. The solvent-dependent phosphorescence lifetime measurements (Figure S6) gave an excellent trend for **4I−Au**; the polarity of the solvent increases except in the case of hexane: toluene (82 μs) > THF (72 μs) > DCM (65 μs) > DMF (44 μs) > MeCN (34 μs) > EtOH (25 μs) > MeOH (19 μs). The solvent-dependent ordering was also confirmed for **4Br−Au**: THF (64 μs) > toluene (53 μs) > DCM (41 μs) > DMF (38 μs) > MeCN (23 μs) > EtOH (21 μs) > MeOH (16 μs); for **4CF$_3$−Au**: toluene (28 μs) > DCM (20 μs) > THF (19 μs) > DMF (13 μs) > EtOH (12 μs) > MeCN (11 μs) > MeOH (9 μs).

Computational Studies. Computational studies were performed with the Amsterdam Density Functional (ADF) 2019 suite of programs. Ground state geometries were calculated in B3LYP-D3 functional and the Slater type DZP basis without frozen core. Zeroth-order regular approximation (ZORA) with a scalar level of relativistic effect was applied for heavy atom calculations. A TZP basis set was used in single point calculation of optimized structures.

4Br−Au and **4I−Au** exhibited emission intensity increases with temperature unlike **4CF$_3$−Au**. To better understand TADF for the three gold corroles, TDDFT calculations were conducted (Figure 3). The rate constants of ISC and rISC were evaluated using Marcus theory (Table S1). $\langle S_1|\hat{H}_{SO}|T_1\rangle$ is the spin−orbit coupling matrix element (SOCME) between S_1 and T_1 states; ΔE is the energy difference between the S_1 and T_1; and the λ_M means the Marcus reorganization energy.

https://doi.org/10.1021/acs.inorgchem.1c00906
Inorg. Chem. 2021, 60, 8442−8446

All corroles showed the strong spin−orbit coupling value between S_1 and T_1, due to the presence of heavy atoms.

TDDFT calculations yielded a very fast intersystem crossing rate constant of 10^{11} to 10^{12} s^{-1}. However, **4CF$_3$−Au** shows a much lower rate constant of rISC of 10^{-8} s^{-1}. **4Br−Au** and **4I−Au** show rate constants of 10^3 and 10^7 s^{-1}, respectively. The much lower rate constant of rISC of **4CF$_3$−Au** was to be expected: a large energy difference exists between the S_1 and T_1 states. **4I−Au** possessed the smallest value of ΔE over other gold corroles, with a value of 0.448 eV, and also showed the largest rate constant of rISC. Only in the case of **4CF$_3$−Au** is the up-conversion from the triplet excited state to the singlet excited state not allowed because of the high energy differences between S_1 and T_1.

We explored the β-tetra-substituted gold corrole platform. The tetra-iodinated gold corrole **4I−Au** exhibited the greatest absorption red shift, whereas **4CF$_3$−Au** showed the most red-shifted room temperature phosphorescence spectrum (λ_{em} = 858 nm, toluene). Delayed fluorescence emission was observed for complexes **4I/Br−Au** and examined via temperature-dependent emission measurements (delayed thermal fluorescence, DTF), showing emission peaks at 628 and 640 nm, respectively. A negative linear relationship between the Soret bands of corroles **4I/Br−Au** and the polarizability function $F(n)$ suggests that the excited states of **4I/Br−Au** are more polar than their ground states. Solvent dependence in the phosphorescence intensity and corresponding lifetimes was also observed: a general decline in phosphorescence intensity was observed with increasing solvent polarity. ISC and rISC values were calculated by the TDDFT study; all gold corroles showed very large ISC rate constants. In contrast, **4CF$_3$−Au** showed a rISC rate constant of almost zero (unit of 10^{-8} s^{-1}), different from those of **4Br−Au** and **4I−Au** (10^3 s^{-1} and 10^7 s^{-1}, respectively).

■ ASSOCIATED CONTENT

Supporting Information

The Supporting Information is available free of charge at https://pubs.acs.org/doi/10.1021/acs.inorgchem.1c00906.

Experimental and computational details, spectra, MO diagrams, energy diagrams, geometry coordinates (PDF)

■ AUTHOR INFORMATION

Corresponding Authors

Atif Mahammed − *Schulich Faculty of Chemistry, Technion−Israel Institute of Technology, Haifa 320000, Israel*; Email: chatif@technion.ac.il

David G. Churchill − *Schulich Faculty of Chemistry, Technion−Israel Institute of Technology, Haifa 320000, Israel; Department of Chemistry, Korea Advanced Institute of Science and Technology (KAIST), Daejeon 34141, Republic of Korea; Therapeutic Bioengineering Section, KAIST Institute for Health Science and Technology (KIHST), Daejeon 34141, Republic of Korea; Center for Catalytic Hydrocarbon Functionalizations, Institute for Basic Science (IBS), Daejeon 34141, Republic of Korea*; orcid.org/0000-0002-2520-4638; Email: dchurchill@kaist.ac.kr

Zeev Gross − *Schulich Faculty of Chemistry, Technion−Israel Institute of Technology, Haifa 320000, Israel*; Email: chr10zg@technion.ac.il

Authors

Xuan Zhan − *Schulich Faculty of Chemistry, Technion−Israel Institute of Technology, Haifa 320000, Israel;* Present Address: School of Life and Health Sciences, The Chinese University of Hong Kong, Shenzhen (CUHK-Shenzhen), 2001 Longxiang Blvd., Longgang Dist., Shenzhen, Guangdong, 518172, P. R. China (X.Z.).

Woohyun Lee − *Department of Chemistry, Korea Advanced Institute of Science and Technology (KAIST), Daejeon 34141, Republic of Korea;* Present Address: Global Infra Technology, Samsung Electronics, 1 Samsungjeonja-ro, Hwaseong-si, Gyeonggi-do 18448, Republic of Korea (W.L.).

Kolanu Sudhakar − *Schulich Faculty of Chemistry, Technion−Israel Institute of Technology, Haifa 320000, Israel*

Donghyeon Kim − *Department of Chemistry, Korea Advanced Institute of Science and Technology (KAIST), Daejeon 34141, Republic of Korea*; orcid.org/0000-0003-1654-649X

Complete contact information is available at: https://pubs.acs.org/10.1021/acs.inorgchem.1c00906

Notes

The authors declare no competing financial interest.

■ ACKNOWLEDGMENTS

Z.G. acknowledges support from the Israel Science Foundation. D.G.C. acknowledges Z.G., the Schulich Faculty of Chemistry, Technion-Israel Institute of Technology, and support from KAIST for facilitating his sabbatical year (2017−2018). W. L. and D. K. gratefully thank the laboratory of Professor Mu-hyun Baik (Department of Chemistry, KAIST and IBS) for cooperation in carrying out theoretical calculations. D.G.C. acknowledges the KAIX program (KAIST), and Professors Hee-Seung Lee and Young-Min Rhee for financial assistance during the fiscal years of 2020 and 2021.

■ REFERENCES

(1) (a) Barata, J. F. B.; Neves, M. G. P. M. S.; Faustino, M. A. F.; Tome, A. C.; Cavaleiro, J. A. S. Strategies for Corrole Functionalization. *Chem. Rev.* **2017**, *117*, 3192−3253. (b) Teo, R. D.; Hwang, J. Y.; Termini, J.; Gross, Z.; Gray, H. B. Fighting Cancer with Corroles. *Chem. Rev.* **2017**, *117*, 2711−2729. (c) Orlowski, R.; Gryko, D.; Gryko, D. T. Synthesis of Corroles and Their Heteroanalogs. *Chem. Rev.* **2017**, *117*, 3102−3137. (d) Aviv, I.; Gross, Z. Corrole-based Applications. *Chem. Commun.* **2007**, 1987−1999. (e) Lemon, C. M. Corrole photochemistry. *Pure Appl. Chem.* **2020**, *92*, 1901−1919.

(2) (a) Nardis, S.; Mandoj, F.; Stefanelli, M.; Paolesse, R. Metal complexes of corrole. *Coord. Chem. Rev.* **2019**, *388*, 360−405. (b) Ghosh, A. Electronic Structure of Corrole Derivatives: Insights from Molecular Structures, Spectroscopy, Electrochemistry, and Quantum Chemical Calculations. *Chem. Rev.* **2017**, *117*, 3798−3881.

(3) Nigel-Etinger, I.; Goldberg, I.; Gross, Z. 5d Early-Transition-Metal Corroles: a Trioxo-Bridged Binuclear Tungsten(VI) Derivative. *Inorg. Chem.* **2012**, *51*, 1983−1985.

(4) Einrem, R. F.; Gagnon, K. J.; Alemayehu, A. B.; Ghosh, A. Metal−Ligand Misfits: Facile Access to Rhenium−Oxo Corroles by Oxidative Metalation. *Chem. - Eur. J.* **2016**, *22*, 517−520.

(5) (a) Palmer, J. H.; Day, M. W.; Wilson, A. D.; Henling, L. M.; Gross, Z.; Gray, H. B. Iridium Corroles. *J. Am. Chem. Soc.* **2008**, *130*, 7786−7787. (b) Schweyen, P.; Brandhorst, K.; Hoffmann, M.; Wolfram, B.; Zaretzke, M. K.; Broering, M. Viking Helmet Corroles: Activating Inert Oxidometal Corroles. *Chem. - Eur. J.* **2017**, *23*,

13897−13900. (c) Palmer, J. H.; Durrell, A. C.; Gross, Z.; Winkler, J. R.; Gray, H. B. Near-IR Phosphorescence of Iridium(III) Corroles at Ambient Temperature. *J. Am. Chem. Soc.* **2010**, *132*, 9230−9231.
(6) (a) Rabinovich, E.; Goldberg, I.; Gross, Z. Gold(I) and Gold(III) Corroles. *Chem. - Eur. J.* **2011**, *17*, 12294−12301. (b) Thomas, K. E.; Alemayehu, A. B.; Conradie, J.; Beavers, C.; Ghosh, A. Synthesis and Molecular Structure of Gold Triarylcorroles. *Inorg. Chem.* **2011**, *50*, 12844−12851. (c) Sudhakar, K.; Mizrahi, A.; Kosa, M.; Fridman, N.; Tumanskii, B.; Saphier, M.; Gross, Z. Effect of Selective CF_3 Substitution on the Physical and Chemical Properties of Gold Corroles. *Angew. Chem., Int. Ed.* **2017**, *56*, 9837−9841. (d) Kruk, M.; Ngo, T. H.; Verstappen, P.; Starukhin, A.; Hofkens, J.; Dehaen, W.; Maes, W. Unraveling the Fluorescence Features of Individual Corrole NH Tautomers. *J. Phys. Chem. A* **2012**, *116*, 10695−10703. (e) Flamigni, L.; Wyrostek, D.; Voloshchuk, R.; Gryko, D. T. Solvent polarity effect on intramolecular electron transfer in a corrole-naphthalene bisimide dyad. *Phys. Chem. Chem. Phys.* **2010**, *12*, 474−483. (f) Lee, W.; Zhan, X.; Palma, J.; Vestfrid, J.; Gross, Z.; Churchill, D. G. Minding our P-block and Q-bands: paving inroads into main group corrole research to help instil broader potential. *Chem. Commun.* **2021**, *57*, 4605−4641.
(7) Alemayehu, A. B.; McCormick, L. J.; Vazquez-Lima, H.; Ghosh, A. Relativistic Effects on a Metal−Metal Bond: Osmium Corrole Dimers. *Inorg. Chem.* **2019**, *58*, 2798−2806.
(8) Lemon, C. M.; Powers, D. C.; Brothers, P. J.; Nocera, D. G. Gold Corroles as Near-IR Phosphors for Oxygen Sensing. *Inorg. Chem.* **2017**, *56*, 10991−10997.
(9) Teo, R. D.; Gray, H. B.; Lim, P.; Termini, J.; Domeshek, E.; Gross, Z. A Cytotoxic and Cytostatic Gold(III) Corrole. *Chem. Commun.* **2014**, *50*, 13789−13792.
(10) Lai, S. L.; Wang, L.; Yang, C.; Chan, M. Y.; Guan, X. G.; Kwok, C. C.; Che, C. − M. Gold(III) Corroles for High Performance Organic Solar Cells. *Adv. Funct. Mater.* **2014**, *24*, 4655−4665.
(11) (a) Alemayehu, A. B.; Einrem, R. F.; McCormick-McPherson, L. J.; Settineri, N. S.; Ghosh, A. Synthesis and molecular structure of perhalogenated rhenium-oxo corroles. *Sci. Rep.* **2020**, *10*, 19727−19737. (b) Nardis, S.; Mandoj, F.; Paolesse, R.; Fronczek, F. R.; Smith, K. M.; Prodi, L.; Montalti, M.; Battistini, G. Synthesis and Functionalization of Germanium Triphenylcorrolate: The First Example of a Partially Brominated Corrole. *Eur. J. Inorg. Chem.* **2007**, *2007*, 2345−2352. (c) Du, R. B.; Liu, C.; Shen, D. M.; Chen, Q. Y. Partial Bromination and Fluoroalkylation of 5,10,15Tris-(pentafluorophenyl)corrole. *Synlett* **2009**, *2009*, 2701−2705.
(12) (a) Sudhakar, K.; Mahammed, A.; Fridman, N.; Gross, Z. Iodinated Cobalt Corroles. *J. Porphyrins Phthalocyanines* **2017**, *21*, 900−907. (b) Soll, M.; Sudhakar, K.; Fridman, N.; Muller, A.; Roder, B.; Gross, Z. One-Pot Conversion of Fluorophores to Phosphorophores. *Org. Lett.* **2016**, *18*, 5840−5843.
(13) (a) Zhan, X.; Yadav, P.; Diskin-Posner, Y.; Fridman, N.; Sundararajan, M.; Ullah, Z.; Chen, Q. C.; Shimon, L. J. W.; Mahammed, A.; Churchill, D. G.; Baik, M. H.; Gross, Z. Positive Shift in Corrole Redox Potentials Leveraged by Modest β-CF_3-substitution Helps Achieve Efficient Photocatalytic C−H Bond Functionalization by Group 13 Complexes. *Dalton. Trans* **2019**, *48*, 12279−12286. (b) Zhan, X.; Teplitzky, P.; Diskin-Posner, Y.; Sundararajan, M.; Ullah, Z.; Chen, Q.-C.; Shimon, L. J. W.; Saltsman, I.; Mahammed, A.; Kosa, M.; Baik, M.-H.; Churchill, D. G.; Gross, Z. Maximizing Property Tuning of Phosphorus Corrole Photocatalysts through a Trifluoromethylation Approach. *Inorg. Chem.* **2019**, *58*, 6184−6198. (c) Sudhakar, K.; Mahammed, A.; Fridman, N.; Gross, Z. Trifluoromethylation for Affecting the Structural, Electronic and Redox Properties of Cobalt Corroles. *Dalton. Trans* **2019**, *48*, 4798−4810. (d) Tamiaki, H.; Nagata, Y.; Tsudzuki, S. Synthesis of Trifluoromethyl-Porphyrins and -Chlorins. *Eur. J. Org. Chem.* **1999**, *1999*, 2471−2473. (e) Sudhakar, K.; Mahammed, A.; Chen, Q.-C.; Fridman, N.; Tumanskii, B.; Gross, Z. Copper complexes of CF_3-substituted corroles for affecting redox potentials and electrocatalysis. *ACS Appl. Energy Mater.* **2020**, *3*, 2828−2836.
(14) Chen, P.-Y.; Meyer, T. J. Medium Effects on Charge Transfer in Metal Complexes. *Chem. Rev.* **1998**, *98*, 1439−1477.
(15) Kadish, K. M.; Shao, J.; Ou, Z.; Gros, C. P.; Bolze, F.; Barbe, J.-M.; Guilard, R. Alkyl- and Aryl-Substituted Corroles. 4. Solvent Effects on the Electrochemical and Spectral Properties of Cobalt Corroles. *Inorg. Chem.* **2003**, *42*, 4062−4070.
(16) Shen, J.; El Ojaimi, M.; Chkounda, M.; Gros, C. P.; Barbe, J.-M.; Shao, J.; Guilard, R.; Kadish, K. M. Solvent, Anion, and Structural Effects on the Redox Potentials and UV−visible Spectral Properties of Mononuclear Manganese Corroles. *Inorg. Chem.* **2008**, *47*, 7717−7727.
(17) Lu, G. F.; Lin, W. S.; Fang, Y. Y.; Zhu, W. H.; Ji, X. L.; Ou, Z. P. Synthesis and Electrochemical Properties of Meso-phenyl Substituted Copper Corroles: Solvent Effect on Copper Oxidation State. *J. Porphyrins Phthalocyanines* **2011**, *15*, 1265−1274.
(18) Mahammed, A.; Gray, H. B.; Meier-Callahan, A. E.; Gross, Z. Aerobic Oxidations Catalyzed by Chromium Corroles. *J. Am. Chem. Soc.* **2003**, *125*, 1162−1163.
(19) Zhan, X.; Zhao, F.; Zhang, L.; Lu, B. B.; Peng, S. H.; Ying, X.; Wang, H.; Liu, H. Y. Influence of Halogenated Benzene Solvents on the Photophysical Properties of Gallium Corroles: the External Heavy Atom Effect. *Wuli Huaxue Xuebao* **2016**, *32*, 771−779.
(20) Lakowicz, J. R. *Principles of Fluorescence Spectroscopy*, 2nd ed.; Klewer Academic/Plenum Publishers: New York, 1999.
(21) (a) Marcus, R. A. On the Theory of Shifts and Broadening of Electronic Spectra of Polar Solutes in Polar Media. *J. Chem. Phys.* **1965**, *43*, 1261. (b) Mody, V. V.; Fitzpatrick, M. B.; Zabaneh, S. S.; Czernuszewicz, R. S.; Gałezowski, M.ł; Gryko, D. T. Solvent Effects on the Electronic and Vibrational Properties of High-valent Oxomolybdenum(V) 5,10,15-triphenylcorrole Probed by UV-Visible and Resonance Raman Spectroscopy. *J. Porphyrins Phthalocyanines* **2009**, *13*, 1040−1052.
(22) Rauh, R. D.; Leermakers, P. A. Solvent Effects upon the Phosphorescence Lifetimes and Photoreactivity of Butyrophenone. *J. Am. Chem. Soc.* **1968**, *90*, 2246−2249.
(23) Fouassier, J. P.; Jacques, P.; Encinas, M. V. Solvent Effects on the Thioxanthone Triplet Quenching by Vinyl Monomers. *Chem. Phys. Lett.* **1988**, *148*, 309−312.
(24) Cheng, S. B.; Song, P.; Yang, S. Q.; Yin, H. M.; Han, K. L. Fluorescence and Solvent-dependent Phosphorescence Studies Ofo-nitrobenzaldehyde: A Combined Experimental and Theoretical Investigation. *Phys. Chem. Chem. Phys.* **2010**, *12*, 9067−9074.

https://doi.org/10.1021/acs.inorgchem.1c00906
Inorg. Chem. 2021, 60, 8442−8446